

# Shape Modeling for the Analysis of Heart Deformation Patterns

Davide Moroni<sup>1</sup>, Sara Colantonio<sup>1</sup>, Ovidio Salvetti<sup>1</sup> and Mario Salvetti<sup>2</sup>

<sup>1</sup> Institute of Information Science and Technologies (ISTI)  
Italian National Research Council (CNR), Pisa, Italy

<sup>2</sup> Department of Mathematics, University of Pisa, Pisa, Italy

**Abstract.** In this paper, we present an approach to the description of time-varying anatomical structures. The main goal is to compactly but faithfully describe the whole heart cycle in such a way to allow for deformation pattern characterization and assessment. Using such an encoding, a reference database can be built, thus permitting similarity searches or data mining procedures.

## 1 Introduction

In the field of computer vision, analyzing the deformation pattern of non-rigid structures may convey useful information in a variety of settings. For example satellite image sequences display temporal evolution of complex structures like clouds and vortices, whose analysis is essential for meteorological forecast [1]; reinforcement of speech recognition by visual data may also be based on the analysis of lips deformation [2]. More interestingly for our purposes, in medicine, the detection and analysis of organ deformations may shed new light in understanding their functional properties and may convey non trivial support in diagnosis. Deformations inside the body may be inherent to the nature of an organ (e.g. the lungs and the heart) or may be due to physiological/pathological growth of tissues and structures. For example, it has been proven that irregular growth of the hippocampus is strongly correlated to epilepsy; thus analysis of hippocampus deformations through 3D models may be used as a clinical decision support to avoid unnecessary brain surgery [3]. Again, in the field of neurology, simulation of intracranial phenomena such as haemorrhages, neoplasm and hematoma may be used to analyze the influences they have on neuro-functional structures in the brain [4].

Imaging modalities provide an invaluable aid in analyzing such complex structures. However image sequences contain a huge amount of high dimensional data (2 or 3 spatial dimensions plus time) which cannot be fully exploited unless with the help of suitable tools for image processing, pattern recognition and image understanding. Actually, in cardiac analysis, well-established imaging techniques (MRI, fastCT, PET, SPECT, ultrasound, ...) allow to acquire video sequences of the heart, from which its dynamical behavior can be inferred. However, in daily practice, sometimes, physicians extract only the most salient frames from the video sequence (end diastole and systole) and

perform direct comparison among images in the selected subset. Considering the full video sequence, more precise and rich information about the state of the heart can be actually discovered.

In this frame, cardiac modelling provides powerful methods for pattern analysis. An abstract representation of the heart is built and can be instantiated to the particular anatomy under examination, with the aim of extracting shape and functional parameters. In addition, cardiac modelling can enable sophisticated quantitative assessment of heart pathologies, for which up-to-now only semi-quantitative evaluation is used in clinical practice. For example, this is the case of ventricular dyssynchrony, a complex phenomenon whose origins are to be tracked back to electrical conduction disturbances that affect both regional and global function of the heart; dyssynchrony results into inco-ordinate ventricular wall motion due to activation delay. Despite its relevance, the only dyssynchrony marker that has received some consensus is an ECG-derived parameter, which however is poorly correlated to the outcome of resynchronization therapy. It may turn out that cardiac modelling may offer new insight into the problem of dyssynchrony characterization, by conveying novel representation features and suitable tools for their scientific visualization. Ultimately, dyssynchrony characterization may be translated via the extracted features into a statistical pattern recognition problem, thus allowing for new methods of quantification [5].

The main goal of cardiac modelling is to compactly but faithfully describe deformable structure in such a way to allow for deformation pattern characterization and assessment. Such an *encoding* would be useful to build up a reference database for similarity searches or data mining procedures.

Motivated by these problems and extending the works [6], [7] and [8], we first define in some generality, the concept of periodically deforming structures (see section 2 for a precise definition) and we start a methodological approach to their study. Besides providing modules for structures reconstruction (Section 4) and characterization (Section 5), that have their own importance in biomedical applications as automatic tools to speed up diagnosis, the main idea is to define a reference dynamic model of a structure class: this model can be understood as an encoding of morphological and functional properties of a periodically deforming structure during its full deformation cycle (Section 6). In particular, shape changes and evolution of local structure properties are depicted in a concise form in the reference dynamic model, thus allowing for deformation analysis and deformation pattern classification. The methodology is finally applied to the analysis of heart left ventricle in magnetic resonance image sequences.

## 2 Periodically Deforming Structure

A structure  $O$  embedded in the background space  $\Omega \subset \mathbb{R}^d$  ( $d = 2, 3$ ) is a collection

$$O = \{(V^\alpha, P^\alpha)\}_{\alpha=1,2,\dots,k}$$

where each  $V^\alpha$  is a smooth manifold (possibly with boundary) embedded in  $\Omega$  and  $P^\alpha : V^\alpha \rightarrow \mathbb{R}^{d(\alpha)}$  is a smooth *properties function* assuming its values in a suitable properties space.

The smoothness assumption is a quite common hypothesis in computational anatomy

(see e.g. [9]) and it is satisfied in practice to a large extent; it implies for example that differential geometric properties can be computed everywhere. We use, moreover, collection of manifolds -instead of a single one- to be able to describe structure subparts (possibly of different dimensionality) by attaching them specific salient attributes via a dedicated properties function. For example, in heart left ventricle modeling, the structure of interest is the myocardium, that can be modeled as a 3D manifold, whose boundaries are two surfaces: the epicardium and the endocardium. It is convenient to attach to the boundary surfaces a different (actually richer) set of attributes than those used for internal points.

A deforming structure  $\mathcal{O} = (O_t)_{t=0,1,\dots}$  is a temporal sequence of structures satisfying some smoothness constraints. Each  $O_t = \{(V^\alpha, P^\alpha)\}_{1 \leq \alpha \leq k}$  should be regarded as the *snapshot* of the deforming structure at time  $t$ .

We require that each manifold  $V_t^\alpha$  appearing in the snapshot at time  $t$  can be smoothly deformed into  $V_{t+1}^\alpha$  in the subsequent snapshot. Tears or crack of any structure subpart are, therefore, ruled out; moreover, in such a way, we avoid dealing with changes in topology, that would require to model shape transitions. Such a task would be essential for example in meteorological applications, but is far beyond our present scopes in biomedical problems.

Finally, a periodically deforming structure is a deforming structure for which there exists an integer  $T$  such that  $\forall t : O_t = O_{t+T}$ . In other words, the deforming structure depicts a periodic motion; thus, a periodically deforming structure is characterized by a finite list of snapshots  $(O_0, O_1, \dots, O_{T-1})$ , which will be referred to as its deformation cycle.

We make a final assumption about the data available to describe a periodically deforming structure. It is assumed that a sufficiently rich set of synchronous signals and images, possibly from different modalities, has been acquired so as to represent faithfully a physical body or phenomenon of interest. In particular, the data set should include at least one 2D/3D image sequence  $(S_t)_{0 \leq t \leq T-1}$ , from which morphology and regional properties of the structure can be inferred.

### 3 Outline of the Methodology

With the previous assumptions, a reference dynamic model of a structure of interest is constructed by coding the dynamics of the structure in a concise representation of its shape and functional properties.

The approach consists in three modules, each one performing specific tasks. Essentially, the first two modules are dedicated to extract a suitable periodically deforming structure from image data. Then the periodically deforming structure is analyzed and used to construct the reference dynamic model. A more precise outline of the modules used to obtain the aforementioned model is as follows:

**Structure Reconstruction.** For each phase  $t$ , the collection of manifolds  $\{V_t^\alpha\}$  is identified and reconstructed in 2D/3D space by applying neural algorithms to the image sequence  $(S_t)_{1 \leq t \leq T}$ ;

**Structure Characterization.** Morphological features and dynamic descriptors are extracted and coded in a property function  $P_t^\alpha$  that for each point  $x$  of the manifold

$V_t^\alpha$  returns the property vector  $(P_1^\alpha(\mathbf{x}), \dots, P_m^\alpha(\mathbf{x}))$ , where each  $P_i^\alpha$  represents one of the selected features;

**Deformation Pattern Assessment.** Suitable and significant shape descriptors are extracted and spatial distribution of the property functions are evaluated in order to obtain a description of the structure dynamics.

In the following sections, these steps are described in more details.

## 4 Structure Reconstruction

We address the problem of deformable structure reconstruction with a two-stage method, which, firstly, automatically localize the deformable structure and then extracts its finer details, looking for precise contours of the whole structure and of its subparts. To each image  $S_t$ , the following two-stage procedure is applied:

1. *Structure automatic localization:* a cluster analysis, based on the fuzzy  $c$ -means algorithm, is applied to identify and label homogeneous regions in each image. Through a region tracking procedure, the behavior of these regions is analyzed over an entire cycle, in order to extract a rough approximation  $\mathcal{O}' = \{O'_t\}_{0 \leq t \leq T-1}$  of the deformable structure  $\mathcal{O}$ .
2. *Segmentation refinement:*  $\mathcal{O}'$  is used to compute the approximate orientation of the real structure  $\mathcal{O}$ , which, in turn, is used to extract three-dimensional features processed by a dedicated ANN, in order to complete the segmentation, by identifying accurate contours of  $\mathcal{O}$ .

### 4.1 Automatic Localization of Deformable Structures

We assume that shape descriptors of the deformable structure tracked on time exhibit a periodical behavior, with main frequency concentrated in the motion frequency. Further we assume that the subparts of the deformable structures appear as homogeneous regions at some scale. However the latter assumption is dictated by our implementations and can be substituted without altering the spirit of this contribution.

*Clustering.* Homogeneous image regions are first labeled using an unsupervised clustering method, based on the fuzzy  $c$ -means algorithm (FCM) [10]. This algorithm groups a set of data in a predefined number of regions so as to iteratively minimize a criterion function, namely the sum-of-squared-distance from region centroids, weighted by a cluster membership function. A membership grade  $p \in [0, 1]$  is associated to each element of the data set, describing its probability to be in a particular cluster.

The FCM algorithm is applied to each image  $S_t$  to produce a number of clusters: for any voxel  $\mathbf{x}$ , a features vector  $(I_0(\mathbf{x}), I_1(\mathbf{x}), I_2(\mathbf{x}), \dots, I_r(\mathbf{x}))$  is computed so that  $I_0(\mathbf{x}) = S_t(\mathbf{x})$ , and for  $d = 1, \dots, r$ , we set  $I_d(\mathbf{x}) = \mathcal{G}_d * S_t(\mathbf{x})$ , where  $\mathcal{G}_d$  is a Gaussian kernel with standard deviation  $\sigma \propto d$ .

This, in turn, induces a partition of the image domain into a set  $P_t = \{R_t^1, R_t^2, \dots\}$  of disjoint connected regions, where the upper indices  $1, 2, \dots$  are region labels. In the following,  $\rho_t$  will denote the generic region in  $P_t$ .

*Region Tracking.* Once eliminated regions of negligible volume (island removal), an intra-cycle tracking procedure is performed. A simple centroid-based tracking algorithm associates, to any region  $\rho_t \in P_t$  in the phase  $t$ , its correspondent region  $T(\rho_t) \in P_{t+1}$  in the subsequent phase  $t + 1$ . The procedure can be iterated, thus producing a region sequence

$$\rho_t = T^0(\rho_t) \rightarrow T^1(\rho_t) \rightarrow T^2(\rho_t) \rightarrow \dots$$

which may be thought as the evolution of the starting region  $\rho_t$  in the different phases. Considering  $t = 0$  as reference phase, for each  $\rho_t \in P_t$  the regions appearing in its evolution are collected in a list  $\text{Ev}(\rho_0) = (T^t(\rho_0))_{0 \leq t \leq T-1}$ .

*Features Extraction.* For any region  $\rho_0 \in P_0$ , the behavior in time of a shape descriptor  $G$  (such as elementary geometric properties: volume, inertia moments etc. ) can be estimated by evaluating  $G$  for every element in the list  $\text{Ev}(\rho_0)$ , thus obtaining a vector  $f_G(\rho_0) = (G.T_t(\rho_0))_{0 \leq t \leq T-1}$ . We then switch to the frequency domain to detect the oscillatory behavior of  $f_G(\rho_0)$ . Actually, the first harmonic coefficient  $\nu_G(\rho_0)$  in the power spectrum density is selected as a salient feature. Indeed, for fixed regions the variations in  $G$  during time are essentially due to noise; instead for regions in periodic motion the spectrum power is concentrated in the motion frequency. Finally, for a predetermined list  $\{G, H, \dots\}$  of shape descriptors, a features vector  $\mathcal{I}(\rho_0) = (\mu_G(\rho_0), \nu_G(\rho_0), \mu_H(\rho_0), \nu_H(\rho_0), \dots)$  is associated to each  $\rho_0 \in P_0$ .

*Region Classification.* Let  $O'_t$  denote the region corresponding to the deformable structure  $\mathcal{O}$  at the phase  $t$ . At first, the reference phase is considered and  $O'_0$  is searched among regions  $\rho_0 \in P_0$ , taking into account their features vectors  $\mathcal{I}(\rho_0)$ . More precisely, a set of learning examples is used to introduce a Mahalanobis distance in the feature space. Let  $\mathcal{I}_1, \mathcal{I}_2, \dots, \mathcal{I}_s$  be a set of observed feature vectors relative to a training set of regions  $\mathcal{O}'$  with mean  $m$  and covariance matrix  $\Sigma$ . The associated Mahalanobis distance, defined by

$$D(\mathcal{I}) = \left( (\mathcal{I} - m)^t \Sigma^{-1} (\mathcal{I} - m) \right)^{1/2},$$

measures the dissimilarity of a feature vector w.r.t. to the expected region feature vector. Thus, for any new case,  $O'_0$  is selected among candidate regions  $\rho_0 \in P_0$  according to the criterion:

$$O'_0 = \arg \min_{\rho_0 \in P_0} D(\mathcal{I}(\rho_0))$$

In subsequent phases, the region  $O'_t$  is singled out by means of the tracking algorithm, namely  $O'_t$  is defined as  $T^t(O'_0)$ .

## 4.2 Segmentation Refinement

The localization of the deformable structure in the previous section supplies as a byproduct a rough approximation of its boundary surface, which may suffer from poor intensity contrast or the presence of spurious structures. The aim of this stage is to refine the segmentation found in the previous section and to identify as well the contours of the

structure subparts.

The set up is as follows. Let  $\Omega \subset \mathbb{R}^3$  be the image domain of the image  $S_t$ . First we define a features function  $\mathcal{F} : \Omega \rightarrow \mathbb{R}^s$ , that assigns to each point  $\mathbf{x} \in \Omega$  a vector  $\mathcal{F}(\mathbf{x})$  of local features extracted from the image data  $S_t$ . Then we use an approach based on Multi-Level Artificial neural networks (MANN) to find functions  $\Phi_\alpha : \mathbb{R}^s \rightarrow \mathbb{R}$  ( $\alpha = 1, 2, \dots, k$ ) s.t. the level sets:

$$V_\alpha = \{\mathbf{x} \in \Omega \mid \Phi_\alpha(\mathcal{F}(\mathbf{x})) = 0\} \quad \alpha = 1, 2, \dots, k \quad (1)$$

correspond to the surface  $V^\alpha$  respectively.

The functions  $\Phi_\alpha$  are learned using a training set of segmented images and they can be used subsequently to segment new instances.

*Features Extraction* Given an image  $S_t : \Omega \rightarrow \mathbb{R}$ , a features function  $\mathcal{F} : \Omega \rightarrow \mathbb{R}^s$  may be constructed. Since the neural network will eventually use this function for the identification of image edges, it is clear that the function  $\mathcal{F}$  should include edge indicator clues.

The involved features can be divided into two classes. First, low-level features are considered: they are context-independent and do not require any knowledge and/or pre-processing. Some examples are voxel position, gray level value, gradients and other differentials, texture, and so forth. Middle-level features are also selected, since voxel classification can benefit from more accurate clues, specific of the problem at hand. In particular, the knowledge of the deformable structure orientation, obtained as a byproduct in the localization procedure, can be used to individuate an Intrinsic Reference System (IRS) suitable to describe the structure shape. If, in addition, a priori information about the structure shape is available, a reliable clue for detecting edges in the images is given by the gradient along the normal direction to the expected edge orientation. Moreover, a multiscale approach is adopted: the features are computed on blurred images, supplying information about the behavior of the voxel neighborhood, which results in a more robust classification.

*MANN-based Voxel Classification* The set of selected features are processed to accomplish the voxel classification by means of a Multilevel Artificial Neural Network (MANN), which assures several computational advantages [11]. For each voxel  $\mathbf{x}$ , its computed features vector  $\mathcal{F}(\mathbf{x})$  is divided into vectors  $\mathcal{F}^i(\mathbf{x})$ , each one containing features of the same typology and/or correlated. Then each  $\mathcal{F}^i(\mathbf{x})$  is processed by a dedicated classifier based on an unsupervised Self Organizing Maps (SOM) architecture. The set of parallel SOM modules constitutes the first level of the MANN which aims at clustering each portion of the feature vector into crisp classes, thus reducing the computational complexity. Cluster indexes, in turn, are the input of the final decisional level, operated by a single EBP network. The output of this last module consists in the vector  $(\Phi_\alpha(\mathcal{F}(x)))_{1 \leq \alpha \leq k}$  describing voxel membership to the various surfaces  $V^\alpha$  ( $1 \leq \alpha \leq k$ ) according to Equation 1.

The SOM modules are trained according to the Kohonen algorithm [12]. For the EBP module, a set of 3D images should be pre-classified by an expert observer and used for supervised training, performed according to the Resilient Back-Propagation algorithm [13].

## 5 Structure Characterization

The reconstructed structure is further characterized by assigning a significant properties function  $P_t^\alpha : V_t^\alpha \rightarrow \mathbb{R}^{d(\alpha)}$  to each manifold  $V_t^\alpha$ . Three types of properties are considered:

- intensity based properties;
- local shape descriptors;
- local dynamic behavior descriptors.

Examples of properties of the first type are gray level value, gradients, textures and the like. They are extracted from the image sequence  $S_t$  –the one which leads us to structure reconstruction. If data collected from other imaging modalities are available, after performing registration, we can fuse this information to further annotate the structure (for example, in the case of the heart, information regarding perfusion and metabolism, obtained e.g. by means of PET imaging, can be referred to the reconstructed myocardium). Geometric based properties, belonging to the second type, are extracted directly from the collection of manifolds  $\{V_t^\alpha\}$ , and are essential to describe locally the shape of the structure. Again, we may distinguish between context independent features (automatically computable for every manifold of a given dimensionality, such as Gaussian and mean curvature for surfaces) and problem-specific properties.

Finally, the local dynamic behavior may be described by properties borrowed from continuous mechanics (such as velocity field and strain tensor); they, however, require, at least, local motion estimation, that we haven't pursued yet.

## 6 Deformation Pattern Assessment

The aim of this section is to provide methods for the representation of a deformable structure which are suitable for similarity searches and data mining procedures. The main idea is to combine the well established feature vector paradigm for 3D objects (see e.g. [14] for a recent survey) with a modal analysis, able to cope with periodically deforming structures.

Indeed, although the periodically deforming structure obtained in the previous steps can be used in principle to assess the dynamic behavior of the structure and identify its deformation pattern, the voxelwise characterization of the reconstructed structures is not suited for similarity searches. The reason is twofold. First, the given description of the whole structures (collection of manifolds described by functions) has a dimensionality far too high to make the problem computationally feasible. Even worse, the voxelwise characterization does not permit, at least in a straightforward manner, the comparison of anatomical structures belonging to different patients or relative to different phases in the cycle.

We addressed this issue using a deformable model (given for example by mass-spring models as presented in [4] ) and normalizing every instance of anatomical structure to that model: in this way anatomical structures (belonging to the same family) are uniformly described and can be then compared according to the feature paradigm.

To recap, we should look for a new set of ‘more intrinsic’ features  $\mathcal{F}_t$  that should be enough simple and, at the same time, capturing essential information about the structures.

To obtain these new kind of features, global information about the structures can be extracted from the properties function, without introducing any problem-specific model. For example, one may consider the *property spectrum*, that is, by definition, the probability density functions (PDF) of a given component of the property function  $P_t^\alpha(\cdot)$ . This function captures how the property is globally distributed; thus, comparison of different property spectra is directly feasible; to reduce dimensionality, moreover, it could be effective to compute the momenta of the PDF (mean, variance, ...).

However, properties spectrum does not convey any information at all about regional distribution of the property. In clinical applications, this is a drawback which cannot be ignored: actually a small highly abnormal region may not affect appreciably the property spectrum, but its clinical relevance is, usually, not negligible. Hence, spatial distribution of properties has to be analyzed. One approach would be to estimate multidimensional property spectrum [15]. In this way, we may implicitly encode spatial relationship between different kind of features. For example, considering the cords going from the center of mass of a structure to its boundary, we may use the cord length and orientation as a property function defined on the structure boundary. Then, the associated multidimensional PDF implicitly codifies the elongation axis of the structure. A major issue in dealing with such sort of multidimensional shape distributions is the accurate estimation of the PDF. Some methods, based on the fast Gauss transform, have been reported [16]. Although, this approach may be conceivable for general-purpose 3D structure indexing and retrieval, it has low relevance in medical applications, for the too implicit encoding and the scarce characterization capabilities of local abnormal regions. In the same vein, approaches which do not need a refined model of the structure (e.g., Gaussian image, spherical harmonics, Gabor spherical wavelets and other general purposes shape descriptors used for content-based image retrieval) may be suitable. However, in general one should define a model of the structures (whose primitives -elementary bricks- are regions, patches or landmarks) and then propagate it to the set of instances to be analyzed by using matching techniques. It is then possible to consider the average of a property on regions or patches (or its the value in a landmark) as a good feature, since comparisons between averages on homologous regions can be performed straightforwardly.

Following this recipe, a vector of features  $\mathcal{F}_t$  with the desired properties is obtained for each phase of the cycle. The deforming structure is then described by the dynamics of the temporal sequence of feature vectors obtained at different phases of the deformation cycle.

A further fruitful feature transformation may be performed exploiting our assumptions on deformable structures. Indeed, the smoothness of deformations implies that a structure has mainly low frequency excited deformation modes. We extend this slightly assuming that this holds true also for the features lists  $(\mathcal{F}_t)_{1 \leq t \leq T}$ . We assume that the fundamental frequency of the motion is also the main component of each feature tracked on time. With these assumptions, an obvious choice is given by the Fourier transform, followed by a low pass filter, which supplies a new features vector  $\Theta$ .

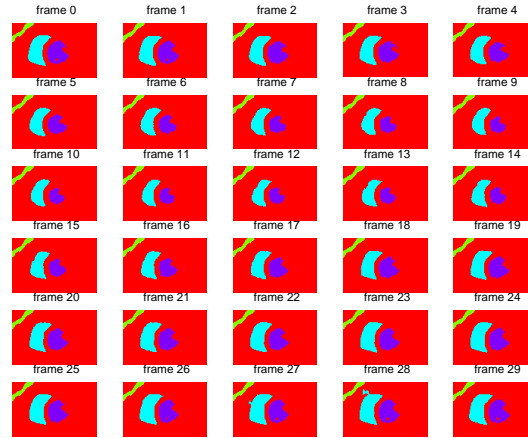


**Fig. 1.** Visualization of the results of clusterization and tracking algorithm (slice number 5).

The evaluation of the above mentioned parameters  $\mathcal{F}_t$ , at each phase  $t$ , implicitly codifies information regarding structure dynamics.

## 7 Case Study: Heart Left Ventricle Analysis

An elective case study for the presented methodology is the analysis of Left Ventricle (LV) that, pumping oxygenated blood around the body, is the part of the heart for which contraction abnormalities are more clinically significant.

The LV structure is modeled as a 3D manifold (the myocardium) with boundary. The boundary has two connected components which are the surfaces corresponding to epicardium and endocardium.

We describe henceforth how the steps of the methodology are applied. First, the deformable structure is extracted from the available data, consisting in a sequence of short axis gradient echo MR images, acquired with the FIESTA, GENESIS SIGNA MRI device (GE medical system), 1.5 Tesla, TR = 4.9 ms, TE = 2.1 ms, flip angle  $45^\circ$  and resolution  $(1.48 \times 1.48 \times 8)$  mm. Sets of  $T = 30$  3D images, consisting of  $k = 11$  2D slices, were acquired at the rate of 30 ms for cardiac cycles [diastole-systole-diastole]. Various clinical cases were considered, for a total of 360 images, corresponding to 12 cardiac cycles. First, FCM was applied separately to each image to produce two clusters using 2 as fuzziness parameter; we considered as a feature vector  $(I_0, I_1, \dots, I_r)$  where  $I_d = \mathcal{G}_d * S_t$  and  $\mathcal{G}_d$  is a gaussian kernel of standard deviation  $d$  times the inslice resolution.

Experimental testing showed that setting  $r = 2$  is sufficient to get a good partition of the image domain. The result of the tracking procedure on a middle slice is shown in Figure 1.

The convex-hull volume and the inertia moments were considered as geometric properties. The use of convex volume (instead of the simpler volume) reduces the effect

of papillary muscles that sometimes move towards the boundary of the region corresponding to the LV. Processing was performed only on middle slices, thus eliminating the apical cap and the basal segments of the LV. Analysis of various clinical cases has been used to introduce the Mahalanobis distance  $D$ ; for simplicity, the covariance matrix  $\Sigma$  has been assumed to be diagonal.

The previously found region corresponds roughly to the LV cavity (LVC) and may be used to introduce an IRS. Since LV is essentially bullet shaped, a hybrid spherical/cylindrical reference system is suitable to characterize its geometry and extract salient edge information. To describe more in detail the IRS, suppose, without loss of generality, that the  $z$ -axis of  $\Omega \subset \mathbb{R}^3$  coincides with the long axis of the LV computed in the previous section and that it is oriented from the apex to the base of the LV. A point  $\mathbf{O} = (0, 0, z_0)$  on the long axis is selected as the switching point between cylindrical and spherical coordinates. Cylindrical coordinates  $(r, \theta, h)$  are assigned to points  $\mathbf{x} = (x, y, z) \in \mathbb{R}^3$  satisfying  $z - z_0 \geq 0$ , whereas spherical coordinates  $(r, \theta, \phi)$  are given to points satisfying  $z - z_0 \leq 0$ . Notice that the unit vector field  $\hat{r}(\mathbf{x}) = \frac{\partial}{\partial r} \mathbf{x} / \|\frac{\partial}{\partial r} \mathbf{x}\|$  (pointing in direction of increasing radial coordinate  $r$ ) is almost orthogonal to cardiac surfaces and, therefore, the derivative  $\frac{\partial S_t}{\partial r}$  along the radial direction may be used as a clue for edge detection. Indeed for a point on a cardiac surface, the modulus of radial derivative is likely to be a high fraction of total gradient magnitude (see Figure 2). Moreover the degree of freedom in the choice of the switching point  $\mathbf{O}$  may be used to tune the IRS to the peculiar cardiac geometry under exam.

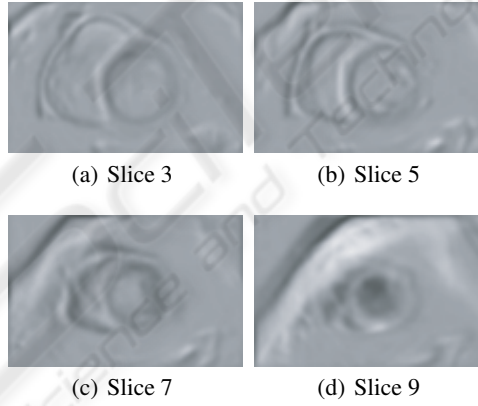


**Fig. 2.** Example of computed features: radial derivative.

The hybrid reference system is used to associate to each point  $\mathbf{x} = (x, y, z) \in \Omega$ , a vector consisting of the following features extracted from the data :

- **Position.** The position of a point  $\mathbf{x}$  w.r.t. the IRS is expressed as a quadruple  $(r, \theta, \phi, h)$ . If  $z - z_0 \leq 0$  the entries  $r, \theta, \phi$  represent its spherical coordinates, whereas  $h$  is set to 0. Similarly, for  $z - z_0 \geq 0$ , the entries  $r, \theta, h$  represent its

cylindrical coordinates whereas  $\phi$  is set to  $\pi/2$ . Notice that with this choice both definitions agree for points in the plane  $z = z_0$ .

- **Intensity.** The intensity value  $S_t(\mathbf{x})$  as well as its smoothed analogues  $\mathcal{G}_d * S_t(\mathbf{x})$ .
- **Gradient norm.** Gradient norm  $\|\nabla(\mathcal{G}_d * S_t(\mathbf{x}))(\mathbf{x})\|$  of the smoothed images  $\mathcal{G}_d * S_t$ .
- **Radial derivative.** The radial derivative of the smoothed images  $\frac{\partial \mathcal{G}_d * S_t(\mathbf{x})}{\partial r}(\mathbf{x}) = \nabla(\mathcal{G}_d * S_t(\mathbf{x})) \cdot \hat{r}$ .

Using the 2-level ANN, voxels are classified on the basis of their features vector as belonging or not to epi- and endocardial surfaces. More in detail, the set of extracted features is divided into two vectors  $\mathcal{F}_1, \mathcal{F}_2$  containing respectively 1) position and intensity and 2) position, gradient norm and radial derivative. The position w.r.t. IRS is replicated in both vectors because it reveals salient for clustering both features subsets. Then, the first level of the MANN consists of two SOM modules, which have been defined as 2D lattice of neurons and dimensioned experimentally, controlling the asymptotic behavior of the number of excited neurons versus the non-excited ones, when increasing the number of total neurons [17].

A  $8 \times 8$  lattice SOM was then trained for clustering the features vector  $\mathcal{F}_1$ , while  $\mathcal{F}_2$  was processed by a  $10 \times 10$  lattice SOM.

A single EBP module has been trained to combine the results of the first level and supply the final response of the MANN. The output layer of this final module consists in two nodes, which are used separately for reconstructing the epicardium and the endocardium. Since each cardiac surface divides the space into two connected regions (one of which is bounded), each output node can be trained using the signed distance function with respect to the relative cardiac surface. In this way, points inside the surface are given negative values, whereas positive values are given to points in the outside. Henceforth the surface of interest correspond to the zero-level set of the output function.

Different architectures have been tested, finding the best performance for a network with only one hidden layer of 15 units. A manual segmentation was performed with expert assistance on the available data. A set of 240 images was used for network training, while the remaining ones were used for network performance test.

The voxel classification, supplied by the MANN, may be directly used for visualization purposes by using an isosurface extraction method, as shown in Figure 3. Figure 4 shows the intersection of the two cardiac surfaces with a slice plane.

Characterization of the reconstructed structure is obtained annotating every voxel with intensity, Gaussian and mean curvature, wall thickness and IRS properties. In particular, Gaussian and mean curvature have been included as shape descriptors whereas wall thickness, which is a classical cardiac parameter, is one example of problem-specific property: it is defined as the thickness of the myocardium along a coordinate ray and it is expected to increase during contraction, since myocardium, being almost water, is, with good approximation, incompressible (see Figure 5).

This characterization is translated into a more amenable form by computing properties spectrum and regional features. In computing spectrum, coordinates w.r.t. IRS have been disregarded, with the exception of radial coordinate; intensity has also been excluded. For any property only mean and variance have been considered. For computing regional features, so far, we used a popular model of the LV (see [18] for a review of 3D-cardiac modelling). In 2D, as shown in Figure 6, it is defined by the intersections of



**Fig. 3.** Different views of the rendered left ventricle at end diastole. The surfaces are obtained applying marching cubes on the two output functions of the network. To eliminate satellites, a standard island removing procedure is applied.

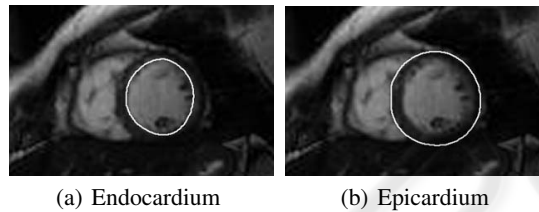


**Fig. 4.** Intersection of cardiac surfaces with a slice plane.

cardiac surfaces with a pencil of equally spaced rays.

The 3D version is obtained by stacking the 2D construction along the axis of the LV. Only 7 middle slices have been considered, giving a total of 168 model points.

The final feature vector  $\Theta$  is obtained taking the first two harmonics of the Fourier transform of the time-sequence  $(\mathcal{F}_t)_{0 \leq t \leq T-1}$ . Since 5 real parameters are required to describe a signal up to second harmonic, the compression ratio is 6 : 1.

## 8 Conclusions and Further Work

In this paper, we have defined a reference dynamic model, encoding morphological and functional properties of a structures class, capable to analyze different scenarios in heart left ventricle analysis. In particular, a framework for the shape characterization and deformation analysis has been introduced for the study of periodically deforming structures.

This framework consists of several modules performing a) structure reconstruction, b) structure characterization, c) pattern deformation assessment. Solutions to specific tasks proposed in each module are, to a large extent, independent and may be combined with other methods, thus broadening the potential application field of the framework. In particular, an approach based on multi-level artificial neural networks has been selected as a general purposes strategy for structure reconstruction, motivated by the promising results presented in [11]. A quantitative evaluation of segmentation performance, based on comparison between images automatically segmented and images annotated by a committee of expert observers, however, is still in progress.

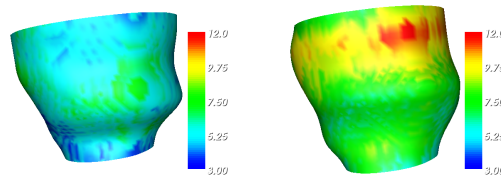


**Fig. 5.** Wall thickness at end diastole and systole, shown as an attribute of epicardial surface. Estimation is performed according to the centerline method and values are expressed in millimeters.

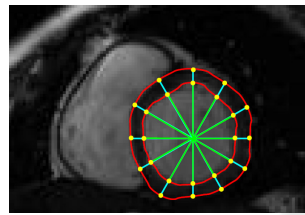


**Fig. 6.** The pencil of equally spaced rays used to computed local features.

The elective case studies are represented by the analysis of heart deformable anatomical structures. Actually, for demonstrating the effectiveness of the proposed framework, we have shown the preliminary results in the study of the heart left ventricle dynamics. The next step will be to employ the obtained results for building up a reference database for similarity searches or data mining procedures.

## Acknowledgements

This work was partially supported by European Project Network of Excellence MUSCLE - FP6-507752 (Multimedia Understanding through Semantics, Computation and Learning) and by European Project HEARTFAID “A knowledge based platform of services for supporting medical-clinical management of the heart failure within the elderly population”(IST-2005-027107).

## References

1. Papin, C., Bouthemy, P., Mèmin, E., Rochard, G.: Tracking and characterization of highly deformable cloud structures. In: Computer Vision - ECCV 2000. Volume 1843 of LNCS., Springer Verlag (2000) 428–442
2. Bregler, C., Konig, Y.: “Eigenlip” for robust speech recognition. In: Acoustics, Speech, and Signal Processing ICASSP-94. Volume II. (1994) 669–672
3. Keim, D.: Efficient geometry-based similarity search of 3D spacial databases. In: Proceedings of the 1999 ACM SIGMOID, New York, ACM Press (1999) 419–430
4. Di Bona, S., Lutzemberger, L., Salvetti, O.: A simulation model for analyzing brain structures deformations. *Physics in Medicine and Biology* 48 (2003) 4001–4022

5. Boyer, K.L., Gotardo, P.F.U., Saltz, J.H., Raman, S.V.: On the detection of intra-ventricular dyssynchrony in the left ventricle from routine cardiac mri. In: ISBI. (2006) 169–172
6. Colantonio, S., Moroni, D., Salvetti, O.: Shape comparison and deformation analysis in biomedical applications. In: Eurographics Italian Chapter Conference. (2006) 37–43
7. Moroni, D., Perner, P., Salvetti, O.: A general approach to shape characterization for biomedical problems. In Perner, P., ed.: Industrial Conference on Data Mining ICDM - Workshop on Mass-Data Analysis of Images and Signals. IBAI CD-Report, Leipzig (2006) 56–65
8. Moroni, D., Colantonio, S., Salvetti, M., Salvetti, O.: Deformable structures localization and reconstruction in 3D images. In Ranchordas, A., Araujo, H., Vitria, J., eds.: 2nd International Conference on Computer Vision Theory and Applications. INSTICC, Barcelona (2007) 215–222
9. Grenander, U., Miller, M.I.: Computational anatomy: an emerging discipline. *Q. Appl. Math.* LVI (1998) 617–694
10. Bezdek, L.: Pattern Recognition with Fuzzy Objective Function Algorithm. Plenum Press, New York (1981)
11. Di Bona, S., Niemann, H., Pieri, G., Salvetti, O.: Brain volumes characterisation using hierarchical neural networks. *Artificial Intelligence in Medicine* 28 (2003) 307–322
12. Kohonen, T.: Self-Organizing Maps. 2nd edn. Volume 30 of Springer Series in Information Sciences. (1997)
13. Riedmiller, M., Braun, H.: A direct adaptive method for faster backpropagation learning: The RPROP algorithm. In: Proc. of the IEEE Intl. Conf. on Neural Networks, San Francisco, CA (1993) 586–591
14. Bustos, B., Keim, D.A., Saupe, D., Schreck, T., Vranic, D.V.: Feature-based similarity search in 3d object databases. *ACM Comput. Surv.* 37 (2005) 345–387
15. Akgül, C.B., Sankur, B., Schmitt, F., Yemez, Y.: Multivariate density-based 3d shape descriptors. In: Shape Modeling International. (2007) 3–12
16. Akgül, C.B., Sankur, B., Yemez, Y., Schmitt, F.: Improving efficiency of density-based shape descriptors for 3d object retrieval. In: MIRAGE. (2007) 330–340
17. Di Bono, M., Pieri, G., Salvetti, O.: A tool for system monitoring based on artificial neural networks. *WSEAS Transactions on Systems* 3 (2004) 746–751
18. Frangi, A.F., Niessen, W.J., Viergever, M.A.: Three-dimensional modeling for functional analysis of cardiac images: A review. *IEEE Trans. Med. Imaging* 20 (2001) 2–5